RSC Advances

ROYAL SOCIETY OF CHEMISTRY

www.rsc.org/advances

RSC Advances

PAPER

Enhancement of icephobic properties based on UV-curable fluorosilicone copolymer films†

Xiaohui Li,[a] Kaiqiang Zhang,[a] Yunhui Zhao,[a] Kongying Zhu,[b] Xiaoyan Yuan,*[a]

DOI: 10.1039/x0xx00000x

www.rsc.org/

UV-curable films composed of thiol-terminated fluorosilicone methacrylate triblock copolymers (PDMS-*b*-(PFMA-SH)$_2$), thiol-functionalized PDMS (PDMS-SH) and octavinyl POSS (OVPOSS) were developed for the purpose of icephobic application. The PDMS-*b*-(PFMA-SH)$_2$ copolymers were firstly synthesized *via* reversible addition–fragmentation chain transfer polymerization of dodecafluoroheptyl methacrylate (12FMA) or 2-perfluorooctylethyl methacrylate (17FMA) and followed thiol-modification of end groups. Results of differential scanning calorimetry and X-ray diffraction revealed that the perfluoroalkyl side groups in P17FMA presented in crystalline structure, that endowed the P17FMA-containing films with higher receding contact angles (100.2–113.5°), as compared with the P12FMA-containing films. In icephobicity investigations of the prepared films, it was found that rebound of impacting droplet was influenced by receding contact angle, surface roughness, and temperature of the film surface. Water droplets could be rebounded from the horizontal and tilted (30° and 45°) P17FMA-containing film surfaces down to -15°C, allowing surfaces dewetting before the water droplets froze, while adhered on P12FMA-containing film surfaces. Moreover, the ice shear strengths on all the prepared film surfaces were lower than 210 kPa, only about 15% of the value on bare aluminum surface. Therefore, P17FMA-containing UV-curable films could be a good candidate for icephobic applications.

1. Introduction

Ice excessive accumulation and adhesion on exposed surfaces may lead to severe accidents and large economic losses.[1,2] Confronted with this problem, icephobic coatings have been developed as a passive technique in decades.[3-5] An ideal icephobic surface should not only repel incoming overcooled water droplets before ice formation, but also reduce ice adhesion on exposed surfaces.[6] Although the superhydrophobic surfaces may have abilities to bounce off incoming droplets and decrease ice adhesion strength,[7-9] water droplet can not rebound and may remain stuck on the surface when the Cassie–Baxter to Wenzel transition occurs.[10,11] In addition, the mechanical interlocking on superhydrophobic surface with a higher surface roughness (usually micron scale) could increase the ice adhesion strength.[12-14] Therefore, hydrophobic coatings with proper surface roughness may exhibit better performance as icephobic materials.

Low surface energy polymer materials, like fluorinated polymers and silicone-based polymers, are often applied to prepare hydrophobic surfaces. Due to the distinguished surface properties, such as low surface free energy and low dielectric constant, fluorinated polymers can be used as icephobic materials,[15,16] whose surface properties depend on the chemical structures of the pendent fluoroalkyl groups. It has been reported that the perfluoroalkyl groups can crystallize due to the side-chain interaction of the fluoroalkyl groups, which is important for stable surface properties.[17-20] Poly(dimethylsiloxane) (PDMS) has also been another widely employed as icephobic material due to its low glass transition temperature (T_g, -123°C) and low surface energy as well. The discrepancy of rheological-mechanical properties between PDMS-based polymer and ice can minimize mechanical interlocking, and reduce ice adhesion strength.[21,22] Fluorosilicone materials, however, integrate the advantages of both fluorinated polymers and silicone-based polymers,[23-25] and create synergistic effects of fluorine and silicon, contributing to the reduction of ice adhesion strength.[26,27]

In the previous reports, we attempted to synthesize fluorosilicone block copolymers *via* free radical polymerization and reversible addition-fragmentation chain transfer (RAFT) polymerization.[28-31] The icephobicity results showed that the ice adhesion strength could be decreased on fluorosilicone block copolymer surfaces indeed, but the water droplets could not rebound from the surfaces and easily result in ice accumulation. It was reported that the rebound of a droplet

[a] *School of Materials Science and Engineering, and Tianjin Key Laboratory of Composite and Functional Materials, Tianjin University, Tianjin 300072, China. Tel. & Fax: 86 22 87401870; E-mail: yuanxy@tju.edu.cn*

[b] *Analysis and Measurement Center, Tianjin University, Tianjin 300072, China*

† Electronic Supplementary Information (ESI) available including compositions of UV-curable films containing fluorosilicone copolymers (Table S1), schematic diagram of water droplets dropping on the sample surface (Fig. S1), FT-IR and ^{1}H NMR spectra of the prepared **S-12F** and **S-17F** block copolymers (Fig. S2; Fig. S3), FT-IR spectra of the **17F10%** film before and after UV curing (Fig. S4), and high speed digital camera images of water droplets dropping on the horizontal or tilted (30° and 45°) sample surfaces at 20°C or -15°C (Fig. S5; Fig. S6; Fig. S7; Fig. S8). Supplementary movies 1-3 show water droplet dropping on the horizontal or tilted (30° and 45°) **17F50%** surface at -15°C. See DOI: 10.1039/x0xx00000x

from a surface is related to the receding contact angle and can be achieved when the receding contact angle is higher than 100°.[32]

In this study, UV-curable films involving fluorosilicone triblock methacrylate copolymers were prepared by UV-curable technique based on thiol-ene functionality. A macro-RAFT chain transfer agent of PDMS with dithiobenzoate groups at both ends (CTA-PDMS-CTA) was initially used for RAFT polymerization of dodecafluoroheptyl methacrylate (12FMA) or 2-perfluorooctylethyl methacrylate (17FMA), which was used as the fluorinated methacrylate monomer (FMA). The dithioester ends of the prepared fuorosilicone triblock copolymers (PDMS-*b*-(PFMA)$_2$) were then transformed into thiol-terminated copolymers (PDMS-*b*-(PFMA-SH)$_2$), and were blended with thiol-functionalized PDMS (PDMS-SH) and octavinyl POSS (OVPOSS) for evaluation as thiol-ene UV-curable systems. The effect of different fluorinated side groups on the wettability and icephobic properties of the prepared UV-curable films was investigated. The PDMS segment in copolymers was designed as the central block for improving the miscibility with PDMS-SH. The PFMA segment was architected at both sides of the copolymer chain for facilitating fluorinated groups to migrate onto surface. The octavinyl POSS (OVPOSS) monomers were used as crosslinking agents. It was hypothesized that the prepared UV-curable fluorosilicone triblock methacrylate copolymer films could enhance the icephobic properties.

2. Experimental methods

2.1 Materials

α,ω-Dihydrogen-terminated poly(dimethylsiloxane) (H-PDMS-H, 4000g/mol) was supplied by Hangzhou Silong Chem-Tech, Hangzhou, China. OVPOSS was purchased from Hybrid Plastics, USA, and used as received. 12FMA were supplied by Xeogia Fluorin-Silicon Chemical Co., Ltd., China. 17FMA, *N*,*N*'-dicyclohexylcarbodiimide (DCC) and 4-dimethylaminopyridine (DMAP) were purchased from Sigma Aldrich. Both 12FMA and 17FMA were purified by passing over a column of alumina to remove inhibitor. 2,2'-Azobisisobutyrobutyl acrylate (AIBN) was obtained from Tianjin Kemiou Chemical Reagent Co., Ltd., China, and used after recrystallization by ethanol. PDMS-SH (2.7 wt% of thiol content, M_n=6000) was obtained from Shanghai Winner Silicone Materials Co., Ltd., China. Dimethylphenylphosphine (Me_2PPh) was obtained from Aladdin Industrial Inc., China. Photoinitiator of 2,2-dimethoxy-2-phenylacetophenone (DMPA) and α,α,α-trifluorotoluene (TFT) were purchased from J&K Chemical Ltd., China, and used as received. Hydrazine hydrate (N_2H_4), tetrahydrofuran (THF), and methanol were supplied by Tianjin Kemiou Chemical Reagent Co., Ltd., China, and used without further purification.

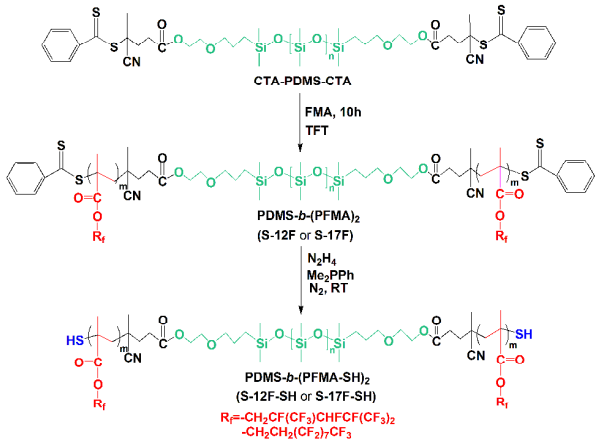

Scheme 1 Synthesis of PDMS-*b*-(PFMA)$_2$ and PDMS-*b*-(PFMA-SH)$_2$ copolymers.

2.2 Synthesis of fluorosilicone triblock methacrylate copolymers

PDMS-*b*-(PFMA-SH)$_2$ were synthesized *via* RAFT polymerization of 12FMA or 17FMA and subsequent thiol-modification of end groups (Scheme 1). The detailed compositions and molecular weights of the prepared triblock copolymers are shown in Table 1.

CTA-PDMS-CTA was prepared by the DCC/DMAP catalyzed esterification of 4-cyanopentanoic acid dithiobenzoate (CPADB) with hydroxyl-terminated PDMS (HO-PDMS-OH),[33] whereas CPADB and HO-PDMS-OH were synthesized according

Table 1 Compositions and molecular weights of the prepared PDMS-*b*-(PFMA)$_2$ block copolymers.

Sample	Structure	[M]:[Macro-RAFT]:[I]	$\overline{M}_{n,NMR}$ (×10^4)	$\overline{M}_{n,GPC}$ (×10^4)	DP_n [a] (FMA)	W_F [b] (wt%)	PDI [c]
–	CTA-PDMS-CTA	–	0.41	0.60	–	–	1.25
S-12F	PDMS-*b*-(P12FMA)$_2$	30:1:0.2	1.12	1.43	18	0.36	1.09
S-17F	PDMS-*b*-(P17FMA)$_2$	15:1:0.2	1.14	1.00	14	0.39	1.08

[a] Measured by ^{1}H NMR after copolymer was purified.

[b] The fluorine content $W_F = \frac{M_{FMA} \times DP_n}{\overline{M}_{n,NMR}} \times F\%$, where *F*% represents F element content in FMA.

[c] Obtained from GPC.

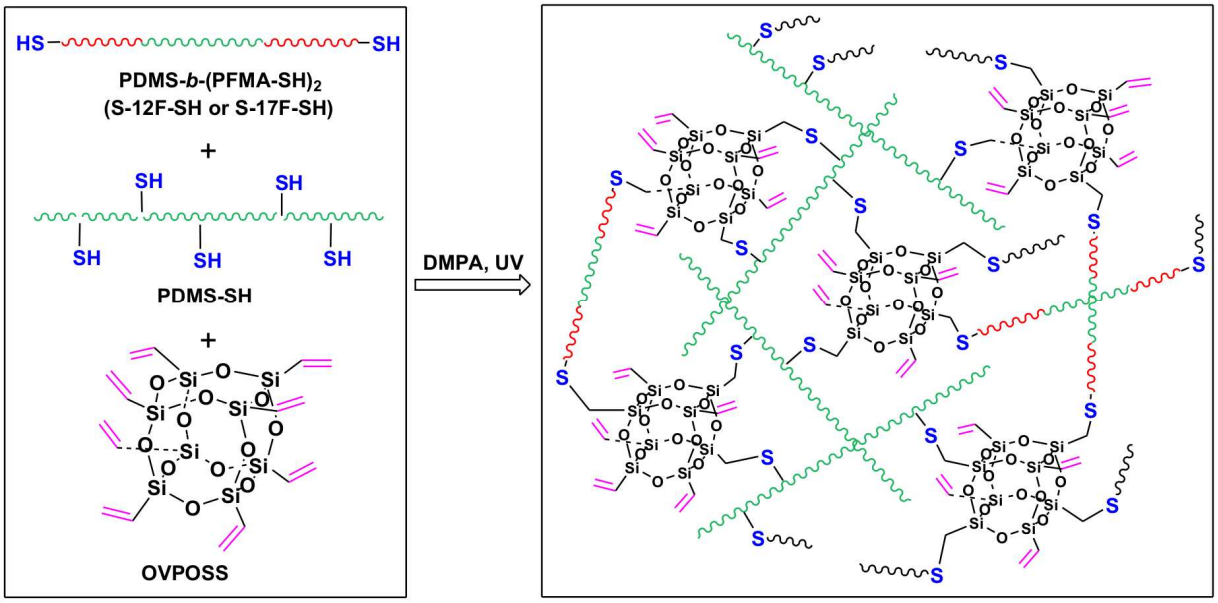

Scheme 2 Preparation of UV-curable fluorosilicone triblock methacrylate copolymer films.

to the references.[34,35] CTA-PDMS-CTA was obtained as red oil-like liquid.

The synthesized CTA-PDMS-CTA was used as macro-RAFT agent to synthesize PDMS-*b*-$(PFMA)_2$ triblock copolymer *via* RAFT polymerization. The polymerization of FMA (12FMA or 17FMA) using AIBN as initiator proceeded with initial molar ratio of each component of [M]:[Macro-RAFT]:[I] = (30 or 15):1:0.2. In a typical experiment, CTA-PDMS-CTA (0.25 g, 0.06 mmol), FMA [12FMA (0.75 g, 1.88 mmol) or 17FMA (0.5 g, 0.93 mmol)] and AIBN (2.0 mg, 0.0125 mmol) were dissolved in 1.0 mL of TFT and placed in a 25 mL Schlenk tube which was thoroughly deoxygenated by three consecutive freeze-pump-thaw cycles. The tube was subsequently placed in an oil bath (70°C for the polymerization of 12FMA, and 80°C for the polymerization of 17FMA) for 10 h. The reaction was stopped by plunging the tube into liquid nitrogen. The reaction mixture was diluted with TFT and poured into an excess volume of methanol to precipitate the polymer product. After several cycles of the dissolution and re-precipitation process, the PDMS-*b*-$(PFMA)_2$ triblock copolymer was purified, and then dried in a vacuum oven overnight. The products are designated as **S-12F** and **S-17F** for PDMS-*b*-$(P12FMA)_2$ and PDMS-*b*-$(P17FMA)_2$, respectively.

PDMS-*b*-$(PFMA\text{-}SH)_2$ was prepared by aminolysis of the PDMS-*b*-$(PFMA)_2$ triblock copolymer. Typically, **S-17F** (0.6 g, 0.053 mmol), N_2H_4 (0.027 mL, 0.53 mmol) and Me_2PPh (0.015 ml, 0.11 mmol) were dispersed in 30mL THF. The polymer solution was stirred under N_2 protection for 5 h at room temperature. During this period, the originally red solution turned colorless. After reaction, the solvent was precipitated into methanol and dried under vacuum. The products are designated as **S-12F-SH** and **S-17F-SH** for PDMS-*b*-$(P12FMA\text{-}SH)_2$ and PDMS-*b*-$(P17FMA\text{-}SH)_2$, respectively.

2.3. Preparation of UV-curable films

The UV-curable films consisted of **S-12F-SH** (or **S-17F-SH**), PDMS-SH and OVPOSS were prepared by UV-curable technique (Scheme 2). The detailed compositions of UV-curable films were listed in Table 2. The UV-curable films are designated as ***x*Fy%,** with varied contents of the thiol-terminated fluorosilicone triblock copolymer in the films (*x*=12 and 17; *y*=1, 3, 5, 10, 20, 30, 40, 50 and 60 wt% copolymer with respect to PDMS-SH). In a typical preparation of **17F10%**, PDMS-SH (1.0 g, 0.17 mmol), OVPOSS (0.1 g, 0.16 mmol), **S-17F-SH** (0.1 g, 0.01 mmol) and DMPA (0.01 g, 0.04 mmol) were dissolved in THF at a concentration of 20 wt%. The UV-curable films were prepared by spin-coating the solutions on polished aluminum plates (20 mm × 20 mm) and irradiated with a 365 nm light (power output 2.5 mW/cm^2, Spectronics, US) for 15 min. Meanwhile, a UV-curable film containing PDMS-SH and OVPOSS without any block copolymers (**F0%**) was also prepared as a control. The film thickness was estimated to be ~0.5 μm by a thickness measurement with atomic force microscopy (AFM).[36]

2.4. Characterizations

Fourier transformed infrared spectroscopy (FT-IR) spectra of samples were recorded in a Spectrum 100 FT-IR spectrometer (Perkin-Elmer, USA) in the range from 4,000 to 500 cm^{-1} using KBr pellet technique. Proton-nuclear magnetic resonance (^{1}H NMR) analysis was carried out in Varian machines (INOVA 500 MHz and Infinity plus 300WB, USA) by dissolving the samples in deuteriochloroform.

UV-vis spectra were recorded on an ultraviolet-visible spectroscopy (UV-2450, Shimadzu, Japan). The average relative molar mass and its distribution of polymers were

determined in gel permeation chromatography (GPC, TDA305, Malvern Instruments Ltd., UK) calibrated by a polystyrene standard with THF as the eluent at a flow rate of 1.0 mL/min under 40°C.

Differential scanning calorimetry (DSC) was measured with a Diamond differential scanning calorimeter (NETZSCH DSC 200 F3, Germany). All data were collected during a second heating run at a scanning rate of 10°C min^{-1} from -150°C to 150°C under a dry nitrogen atmosphere, after heating the samples to 150°C and then quenched to -150°C using liquid nitrogen. X-ray diffraction (XRD) patterns were recorded in a D/max 2500 machine using a wavelength λ = 0.154 nm and a scattering angle 2θ = 3–50°.

Bulk copolymer morphologies were viewed under a transmission electron microscope (TEM) (Tecnai G2 F20 200 kV, the Netherlands), which were prepared by directly dropping of a drop of 1 wt% copolymer solution in THF on the carbon-coated copper grids.

AFM images were obtained using tapping mode at room temperature on a CSPM5500A of Being Nano-Instruments Ltd., Guangzhou, China, equipped with E-type vertical engage piezoelectric scanner.

Surface composition by X-ray photoelectron spectroscopy (XPS) was investigated using a Perkin-Elmer PHI 5000C ECSAX-ray photoelectron spectroscopy in ultra-high vacuum with Al K radiation (1486.6 eV) operating at 24.2 W under a vacuum less than 5×10^{-8} Torr at 45°. The tested area was a circle with diameter of 100 μm.

Water contact angles and contact angle hysteresis of the copolymers and the UV-curable films were measured by an optical contact angle meter (JC2000D, Shanghai Zhongchen Equipment Ltd., China) at room temperature and ambient humidity. The measurement of contact angle hysteresis was carried out using 5 μL water droplets which expanded and shrunk by 10 μL at 0.1-1.0 μL/s *via* a needle from a syringe. Images of the droplets were captured by a CCD camera and analyzed to obtain the advancing and receding contact angles, and values of the water contact angle hysteresis were calculated. The surface energies of the copolymers and the UV-curable films were evaluated by measuring static water and hexadecane contact angles on the surfaces. A drop of the probe liquid (deionized water or hexadecane) in 5 μL was used. The surface energies were calculated according to the equation by Owens–Wendt–Kaelble method.[37] All the contact angles presented are average of five measurements.

The impact experiments of water droplets were conducted using the apparatus illustrated schematically in Fig. S1. The coated Al plate (20 mm×20 mm) was placed onto the horizontal or tilted (30° and 45°) cooling stages. A syringe (50 μL) with pointy needle was fixed above coated Al plate. The distance between the needle tip and coated Al plate was 10 cm. The water was cooled in refrigerator as the source of 0°C water. The cooling stage could be maintained at -15°C, -25°C and -35°C, respectively, in a transparent chamber which was purged with nitrogen to decrease the humidity. Relative humidity inside the chamber was controlled to be less than 20% by flowing of dry nitrogen during the cooling period to minimize frost formation on the samples. During the impact experiment, a water droplet (7 μL) at room temperature or 0°C was dropped onto the sample surface. The whole impacting process was recorded using a high speed camera (Olympus i-SPEED LT 4GB Color, Japan) operated with a frame speed of 1000 frames per second (fps) and an image resolution of 800 × 600 pixels.

The ice shear strength tests were performed using a custom-made cooling stage described in our previous work.[30] Briefly, samples, i.e., the Al plate (20 mm×20 mm) coated by the copolymers, were placed onto the cooling stage. The glass column was put on the Al plate and filled with 450μL of fresh deionized water. The temperature of the stage reached to -15°C at a rate of 2°C/min and was maintained for 3 h. A force transducer (Imada ZP-500 N, Japan) was mounted on a motion stage which moved forward at a rate of 0.5 mm/s to the glass columns. The maximum force was recorded for calculating the ice shear stress by a force transducer which was mounted on a motion stage. All the presented values are averages of at least eight or nine measurements for each specimen.

3. Results and discussion

3.1. Synthesis and characterization of fluorosilicone triblock methacrylate copolymers and UV-curable films

FT-IR and ^{1}H NMR spectra of **S-12F** and **S-17F** block copolymers are shown in Fig. S2 and Fig. S3, respectively. The FT-IR spectra suggested that 12FMA and 17FMA had been incorporated into the fluorosilicone triblock methacrylate copolymers. The degree of polymerization (DP_n) of P12FMA and P17FMA in the prepared copolymers were calculated by comparing the characteristic integral intensities of P12FMA (5.2–6.6 ppm) and P17FMA (2.2–2.6 ppm) with PDMS (0.1 ppm). The calculated values of DP_n as well as the molecular weight ($\overline{M}_{n,\mathrm{NMR}}$ and $\overline{M}_{n,\mathrm{GPC}}$), fluorine content ($W_F$) and polydispersityindex (PDI) of the block copolymers were summarized in Table 1. It can be seen that the values of W_F of the copolymers were almost the same and the PDI were in the range of 1.09–1.24, indicating that the copolymerization proceeded in a controlled manner.

The thiol-terminated fluorosilicone triblock methacrylate copolymers could be confirmed using a combination of UV-vis spectrophotometry and GPC. Fig. 1 exhibits the UV-vis spectra and GPC traces (inset) of **S-12F** and **S-17F** block copolymers and their thiolated products. It could be seen that, after aminolysis, the absorption of C=S bond (~300 nm) disappeared and no shoulder peak was found in GPC traces, indicating the complete transformation of the thioester groups into the thiol groups.[38]

The absorbance change in the FT-IR spectra for the thiol group of **17F10%** before and after UV-curing is depicted in Fig. S4. Disappearance of peak at 2580 cm^{-1} reveals that the S–H group had reacted during the photo-curing polymerization.

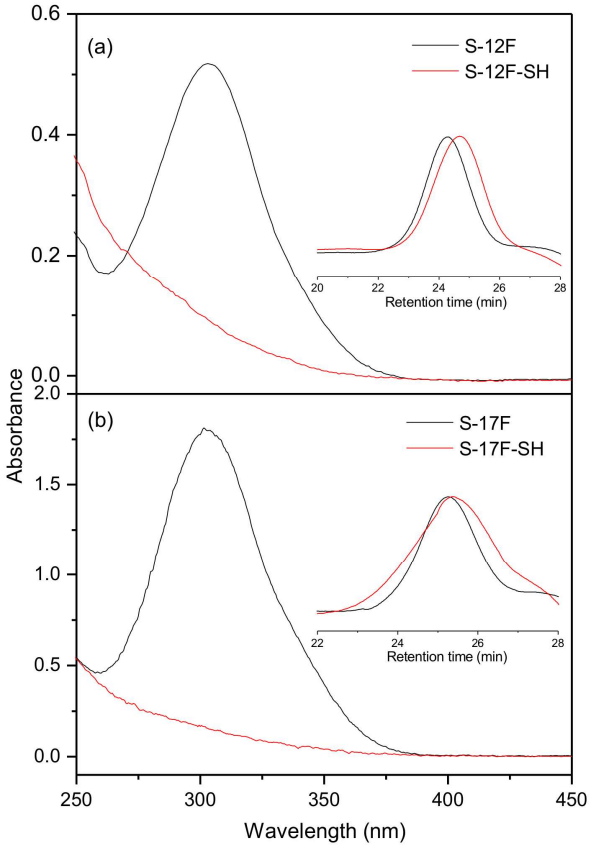

Fig. 1 UV-vis spectra and GPC curves of (a) **S-12F**, **S-12F-SH** and (b) **S-17F**, **S-17F-SH** block copolymers.

3.2. Thermal study and crystalline structure of fluorosilicone triblock methacrylate copolymers and UV-curable films

The thermal transitions of **S-12F** and **S-17F** block copolymers were investigated by DSC (Fig. 2). It could be seen that PDMS had a glass transition temperature (T_{g1}) at -125°C, and in the DSC curve of **S-12F**, a T_{g2} of the P12FMA chain was about 50°C. A peak around 80°C, which was observed in **S-17F**, attributed to the melting of a crystalline structure formed by the perfluoroalkyl side groups.[17,19]

In order to confirm the crystallization of the perfluoroalkyl side groups, the block copolymers and the films were further characterized by XRD. Fig. 3 shows the XRD patterns of **F0%**, **S-12F**, **12F50%**, **S-17F** and **17F50%**. The diffraction peak at 2θ=17°, which was observed in copolymer **S-17F** and film **17F50%**, corresponded to the interside-chain interference from the hexagonal packing of perfluoroalkyl side chains, indicating a crystalline structure of perfluoroalkyl groups in P17FMA segments.[19] At the same time, a crystalline peak at 2θ=9.8°, corresponding to the diffraction of OVPOSS content, was observed in **F0%**, **12F50%**, and **17F50%**. The diffraction at 2θ=9.8° suggests that aggregation of OVPOSS occurred in the films due to the lower miscibility between OVPOSS and

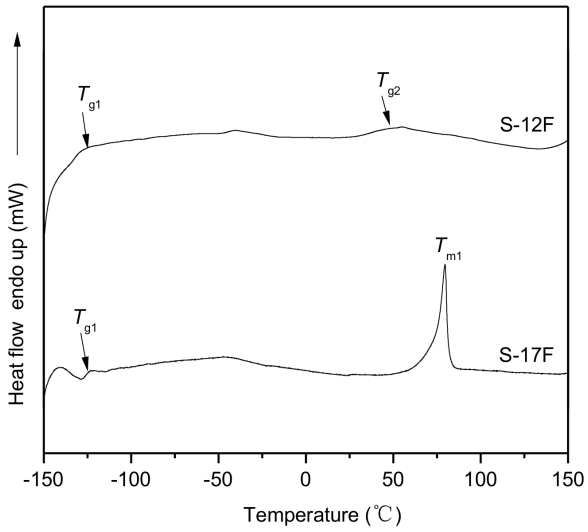

Fig. 2 DSC curves of of **S-12F** and **S-17F** block copolymers.

PDMS-SH.[39] DSC and XRD results reveal that the perfluoroalkyl side groups in P17FMA segments can form crystalline structure, while fluoridated groups in P12FMA segments were not crystallized.

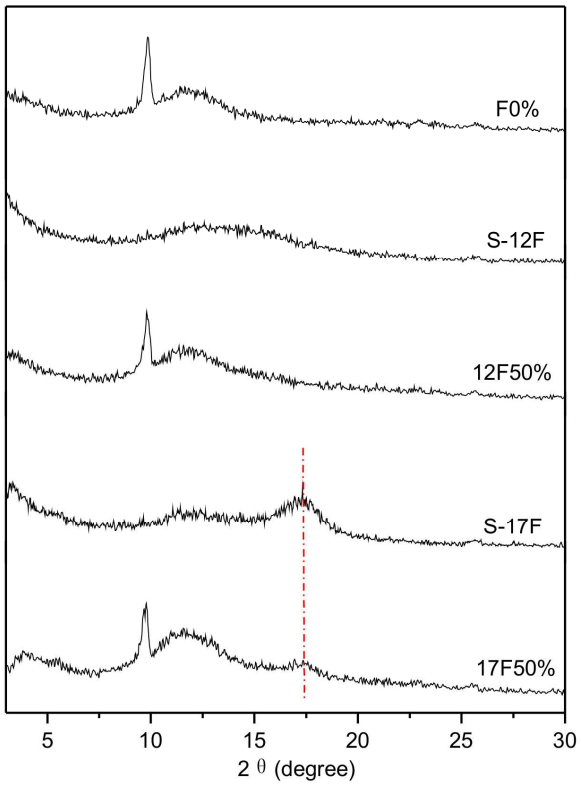

Fig. 3 XRD curves of block copolymers (**S-12F**, **S-17F**) and UV-curable films (**F0%**, **12F50%**, **17F50%**).

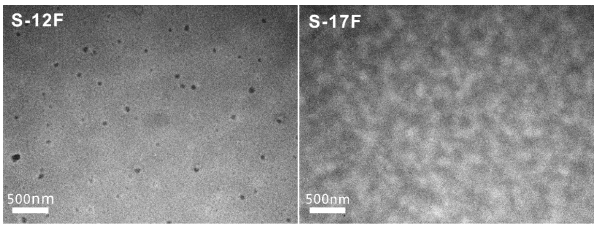

Fig. 4 TEM micrographs of **S-12F** and **S-17F** block copolymers.

3.3. Bulk and surface structure

TEM measurement was conducted on the bulk morphologies of the synthesized block copolymers. As the high electron density of PDMS block, the PDMS blocks appeared as dark regions, while PFMA blocks appeared as bright regions. As shown in Fig. 4, **S-12F** and **S-17F** block copolymers exhibited microphase-separated structures due to the thermodynamic incompatibility between the PDMS and PFMA blocks. The spherical aggregates with diameter approximate 100 nm were clearly seen in **S-12F** because of the high solubility of PDMS and P12FMA segments in THF.[23] However, the domain size of **S-17F** was larger than that of **S-12F** due to higher cohesion of the fluorine component in **S-17F**.[40]

Table 2 Element compositions of block copolymers and UV-curable films obtained by XPS

Sample	C (atomic %)	O (atomic %)	F (atomic %)	Si (atomic %)	F/Si
S-12F	50.4	15.9	24.7	9.1	2.71
S-17F	44.8	11.2	37.4	6.6	5.66
F0%	53.6	24	—	22.4	—
12F1%	49.0	20.9	14.5	15.6	0.93
12F3%	47.6	17.4	22.3	12.7	1.75
12F5%	53.9	17.2	20.1	8.8	2.28
12F10%	48.5	15.8	25.7	10	2.57
12F20%	48.1	16.1	25.4	10.3	2.47
12F30%	44.3	14.7	31.2	9.9	3.15
12F40%	45.7	14.4	29.7	10.2	2.92
12F50%	43.6	16.6	29.1	10.8	2.69
12F60%	46.1	14.8	28.6	10.5	2.73
17F1%	46.3	20.6	18.4	14.6	1.26
17F3%	42.6	16.1	29.1	12.2	2.38
17F5%	43.2	16.6	28.5	11.7	2.43
17F10%	46.6	14.2	29.5	9.7	3.04
17F20%	42.8	13.5	34.4	9.3	3.69
17F30%	41.9	11.6	38.7	7.9	4.9
17F40%	46.0	12.1	34.7	7.2	4.82
17F50%	43.2	12.6	36.0	8.2	4.39
17F60%	49.8	11.4	32.2	6.6	4.88

The XPS measurement was carried out to detect the surface chemical compositions of the block copolymers and the UV-curable films. The carbon, oxygen, fluorine and silicon contents as well as the F/Si ratios are summarized in Table 2. For the block copolymers, the fluorine content on **S-17F** (37.4 wt%) surface was higher than that on **S-12F** (24.7 wt%) surface. For the UV-curable films, the fluorine content on surfaces tended to rise with the increased fluorosilicone block copolymer constitution from 1 to 30 wt%. With the almost same content of block copolymer, the enrichment of fluorine was more significant on the surface of P17FMA-containing films than that of P12FMA-containing ones. For example, the fluorine content on **17F30%** surface (38.7 wt%) was higher than that on **12F30%** surface (31.2 wt%). The higher fluorine content also resulted in high F/Si values on **S-17F** copolymer and P17FMA-containing film surfaces. These results indicate that P17FMA segments with longer fluoridated side groups were easier to move onto the surface than P12FMA segments, even if the crystallization of perfluoroalkyl groups in P17FMA segments would confine the mobility of the molecular chain.

The surface morphologies and roughness of the block copolymers and the films were investigated by AFM in Fig. 5.

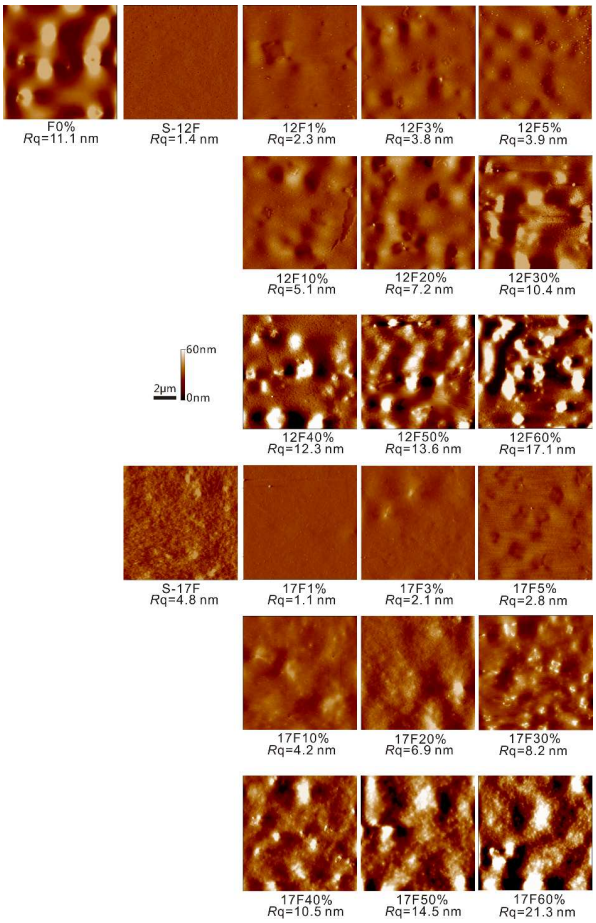

Fig. 5 AFM height images of block copolymers and UV-curable films.

For the copolymers with distinct microphase-separated surface structures, circular concave morphology was formed on the surface **S-12F**, while island type structure was observed on the surface **S-17F**. Taking XPS results into account, the dark areas would represent the PDMS block in **S-12F**, while the bright areas would show the P17FMA domains in **S-17F**. The surface roughness of **S-17F** (4.8 nm) was higher than that of **S-12F** (1.4 nm) due to the enrichment of P17FMA blocks on the surface. For all the P12FMA and P17FMA-containing films, because of the incompatibility of PDMS-SH and fluorine component, the surface roughness increased with the increasing amount of block copolymers. It can be seen that the surface roughness of **17F60%** was 21.3 nm, which was bigger than those of the other films.

3.4. Wettability of films

Fig. 6 shows the water contact angles (a), surface energies (b), receding contact angles (c) and contact angle hysteresises (d) of the block copolymers and the UV-curable films. The water contact angles of **S-17F** (118.6±0.3°) and films with diverse P17FMA content (117.2–118.7°) were higher than those of **S-12F** (105.8±0.3°) and P12FMA-containing films (106.1–107.9°). The surface energies of **S-17F** (10.5 mJ/m^2) and P17FMA-containing films (10.1–10.5 mJ/m^2) were lower than those of **S-12F** (17 mJ/m^2) and P12FMA-containing films (16.7–17.6 mJ/m^2). Moreover, the relatively higher receding contact angles were also found for **S-17F** (112.4±0.3°) and P17FMA-containing films (100.2–113.5°) as compared with **S-12F** (89.6±0.1°) and P12FMA-containing films (92.5-96.7°). This could be attributed to the crystallization of perfluoroalkyl groups in P17FMA segments, which could prevent the surface reorientation in contact with water and enhance segregation of the CF_3 groups on the surface. For **S-12F** and P12FMA-containing films, the polar groups, buried within the surface, were brought out to the surface in contact with water to reduce the surface energy, which is the driving force of this reorientation.[17,18,20]

The contact angle hysteresis which is defined as the difference between the advancing and receding contact angle, is related with surface roughness, heterogeneity and

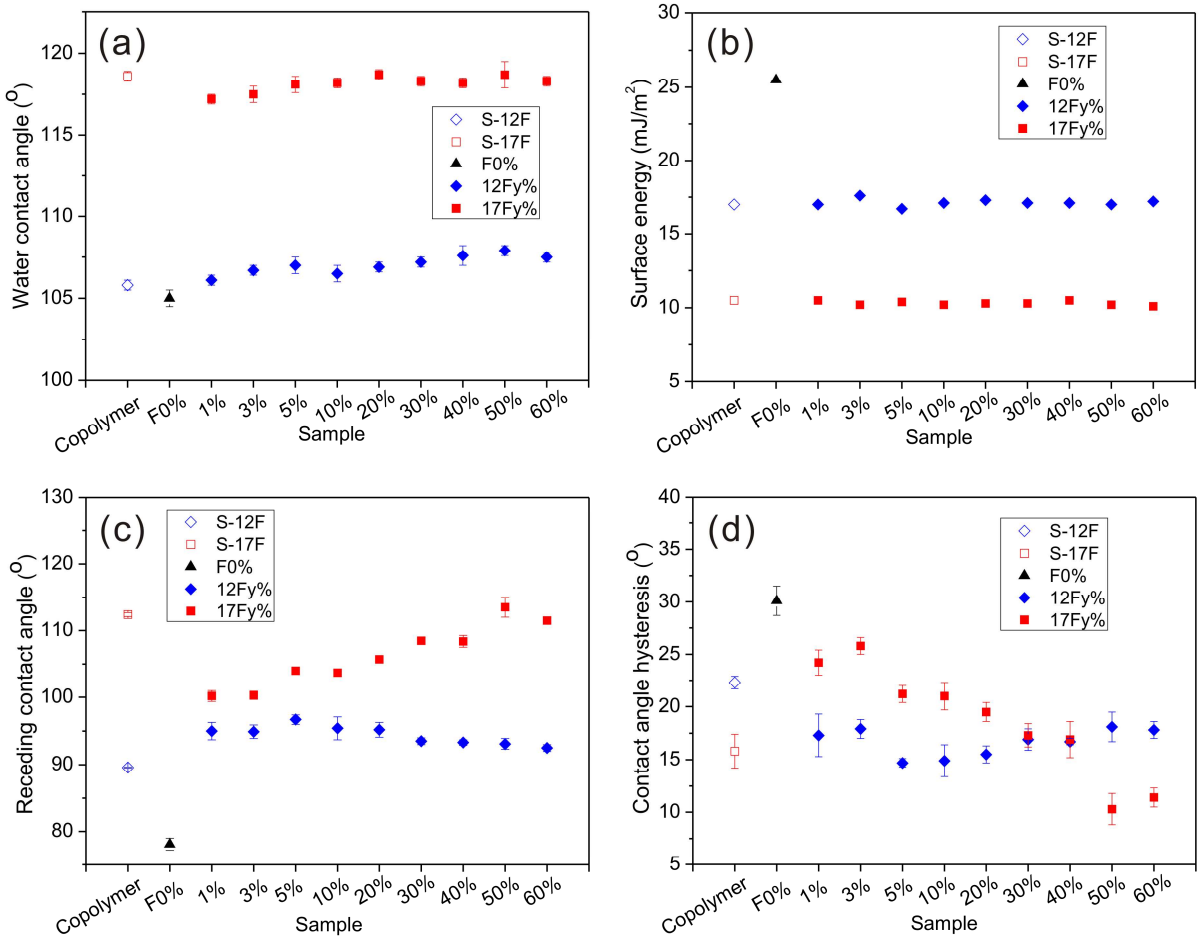

Fig. 6 Water contact angles (a), surface energies (b), receding contact angles (c) and contact angle hysteresises (d) of block copolymers and UV-curable films, y=1, 3, 5, 10, 20, 30, 40, 50, 60.

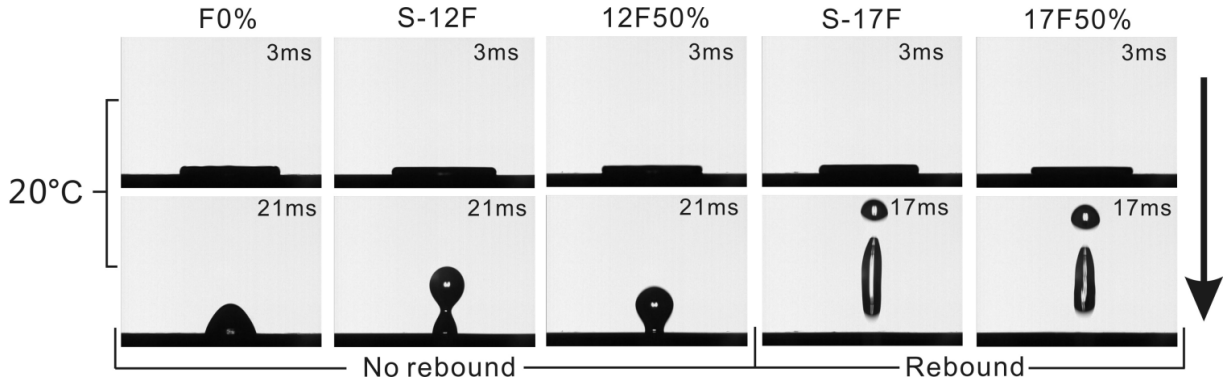

Fig. 7 High speed digital camera images of the dynamic behavior of 7-μL water droplets dropping on the horizontal surface of block copolymers (**S-12F**, **S-17F**) and UV-curable films (**F0%**, **12F50%**, **17F50%**) from a 10 cm height at 20°C.

reorientation.[41] The AFM observation of the copolymer and the UV-curable film surfaces revealed the roughness is small enough (less than 100nm) not to give a large influence on the contact angle hysteresis.[42,43] The contact angle hysteresis of **S-17F** (15.8±1.6°) was lower than that of **S-12F** (22.3±0.6°) due to the crystallization of perfluoroalkyl groups in P17FMA segments. This result indicates that **S-17F** present a more stable liquid repellent state than **S-12F**. However, the contact angle hysteresis of **17F*y*%** (19.5-25.8°) with *y*=1~20% was higher than that of **12F*y*%** (14.7–17.9°) with *y*=1~20%. This could be ascribed to the heterogeneous (having areas of differing surface energies) of **17F*y*%** (*y*=1~20%) surface. As a contrast, **F0%** presented the lowest water contact angle (105±0.5°), highest surface free energy (25.5 mJ/m^2), lowest receding contact angle (78.1±0.9°) and highest contact angle hysteresis (30.1±1.4°) in all the samples due to the lack of fluorocarbon group. For a copolymer or UV-curable film surface containing both fluorocarbon group and siloxane group, the synergistic effect of silicon and fluorine would contribute to the reduction of contact angle hysteresis.[26,27]

3.5. Icephobic properties

3.5.1. Water impact on the copolymer and UV-curable film surfaces

Because the dynamic behavior of a water droplet on a cold surface had great influence on the icephobicity, the water droplet impact tests on the block copolymers and UV-curable films were performed. Fig. 7 displays the dynamic behavior of water droplets (7 μL) dropping on horizontal block copolymer and the film surfaces at 20°C with 10 cm releasing height. It was observed that the **F0%**, **S-12F**, **12F50%**, **S-17F** and **17F50%** surfaces had almost similar water droplet spreading process but different retraction behavior. It can be seen that the water droplets underwent clear retraction on **S-12F** and **12F50%** surfaces, as compared with **F0%**, but did not fully withdraw after that. However, the water droplets could fully withdraw from the **S-17F** and **17F50%** surfaces and rebound after complete retraction. The retraction or rebound behavior of water droplet is related to the receding contact angle. The retraction of droplet is caused by the retraction force, which is a function of the apparent receding contact angle.[44,45] According to the reference,[32] rebound can be observed on surface with receding contact angle higher than 100°. The receding contact angles of **S-12F** (89.6±0.1°) and **12F50%** (93.1±0.8°) were higher than that of **F0%** (78.1±0.9°), which were beneficial for droplet retraction. On **S-17F** and **17F50%** surfaces that had receding contact angles greater than 100° (112.4±0.3° and 113.5±1.5°, respectively), droplet rebound was observed.

In order to investigate the influence of reduced temperature on droplet rebound, a series dynamic droplet experiments at low temperature were conducted. Fig. 8 displays the dynamic behavior of water droplets (7 μL) dropping on the horizontal and tilted (30° and 45°) **17F50%** surface from a 10 cm height at 20°C, -15°C, -25°C and -35°C, respectively. It showed that the water droplet could rebound from the horizontal and tilted (30° and 45°) **17F50%** surface at 20°C and -15°C (see videos in the Supporting Information), allowing surfaces dewetting before the water droplets can actually freeze and avoiding ice accretion, while the water droplet failed to rebound at -25°C and -35°C, which could be attributed to the increased viscosity of water droplet. For droplet impact on substrates at low temperature, the impact event can be affected by the viscous dissipation, since the droplet dissipates more energy through viscous effects during spreading and retracting process.[44,45] Meanwhile, the water droplet showed different impact behavior on **17F50%** surface positioned at different tilted angles. When the temperature was down to -25°C, the water droplet could slip away from surface tilted at 45°, but stick to tilted surface at 30°. This suggests that surface with larger tilted angle would be beneficial for preventing ice accretion. However, for comparison, the water droplet did not fully withdraw and adhered on **12F50%** surface due to its low receding contact angle (Fig. S5).

On the other hand, droplet impact behavior on the horizontal and tilted (30° and 45°) P17FMA-containing film surfaces down to -15°C were also investigated (Fig. S6,

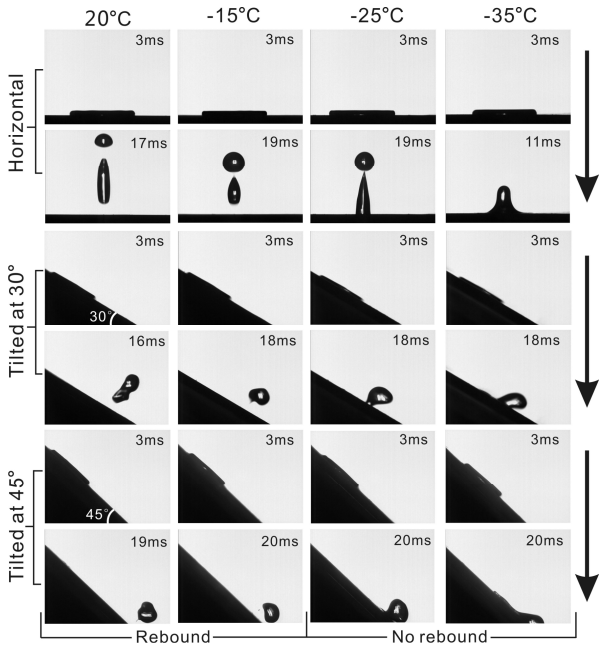

Fig. 8 High speed digital camera images of the dynamic behavior of 7-μL water droplets dropping on the horizontal and tilted (30°, 45°) **17F50%** surface from a 10 cm height at 20°C, -15°C, -25°C and -35°C, respectively.

Fig. S7, and Fig. S8). It can be seen that water droplet could rebound from the film surface when the **S-17F-SH** content below 60%, while could not fully rebound from the horizontal **17F60%** surface and failed to rebound from the tilted (30° and 45°) **17F60%** surface. Based on the AFM results (Fig. 5), the surface roughness of **17F60%** was 21.3 nm, which was bigger than those of the other films. As the surface chemical compositions of **17F50%** and **17F60%** were almost the same (Table 2), the bigger surface roughness of **17F60%** may be the main reason for droplet not fully rebound or failed to rebound, that could result in droplet partially penetrating into the texture. Although superhydrophobic surface is generally considered as a nonwetting surface, the impacting droplet may penetration into the surface texture and do not fully rebound from the surface, resulting in the loss of superhydrophobicity.[10,11,32] Compared with the superhydrophobic surface, the hydrophobic surface (contact angles of 90–120° and receding contact angles higher than 100°) may be more suitable for practical application.

3.5.2. Ice shear strength

The ice shear strength was measured to explore the icephobic property of the copolymers and UV-curable films. Fig. 9 shows the ice shear strengths on the block copolymer and the film surfaces. For comparison, the ice shear strength of bare aluminum was also measured. It could be seen that the ice shear strengths on **F0%** (204±16 kPa), P12FMA-containing (140–210 kPa) and P17FMA-containing films (133–210 kPa) were lower than 210 kPa, only about 15% of the

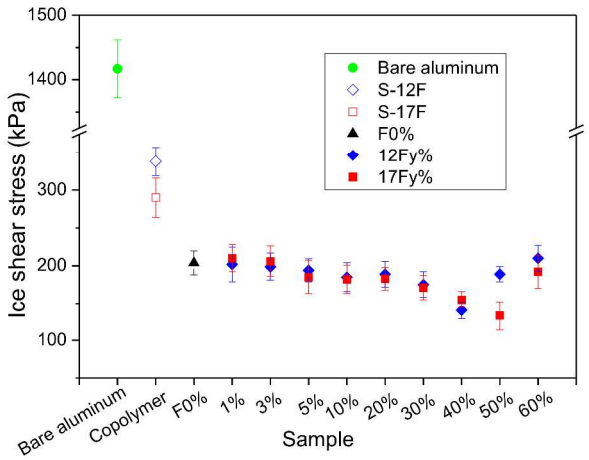

Fig. 9. Ice shear strength of block copolymers and UV-curable films, y=1, 3, 5, 10, 20, 30, 40, 50, 60.

value on bare aluminum surface (1417±139 kPa), and were lower than those on **S-12F** (321±33 kPa) and **S-17F** (290±26 kPa) surfaces. The low ice shear strength on the film surface is mainly attributed to the addition of PDMS-SH, which remains flexible at low temperature due to the low T_g of PDMS and makes UV-curable film more "soft". For UV-curable films, concentrated stress could be built at the ice/film interface, which provides a path for easy ice release.[16,21] The ice shear strengths on UV-curable film surfaces slightly dropped with the increased fluorosilicone copolymer contents due to the synergistic effect of fluorine and silicon, which reduces the interaction between ice and film surface and thus contribute to decreasing the ice shear strength.[26,27] Icephobic tests indicate that the UV-curable fluorosilicone copolymer films, especially for P17FMA-containing UV-curable films which could not only repel incoming water droplets before ice formation but also decrease the ice shear strength, have potential use as icephobic coatings.

4. Conclusions

UV-curable fluorosilicone triblock methacrylate copolymer films were prepared by using thiol-terminated fluorosilicone triblock copolymers (PDMS-*b*-(PFMA-SH)$_2$), which were synthesized *via* RAFT polymerization of 12FMA or 17FMA and subsequent thiol-modification. The effect of different fluorinated side groups on the wettability and icephobic properties of films is discussed. Compared with the P12FMA-containing films, the P17FMA-containing films exhibited higher water contact angles (117.2–118.7°), higher receding contact angles (100.2–113.5°) and lower surface free energies (10.1–10.5 mJ/m^2), because of the crystallization of perfluoroalkyl groups in P17FMA segments. Water droplet impact analysis demonstrated that water droplets could rebound from the horizontal and tilted (30° and 45°) P17FMA-containing film surfaces down to -15°C when the **S-**

17F-SH content below 60%, ascribing to their high receding contact angles. This result indicates that droplets were able to bounce off the P17FMA-containing film surfaces before froze. However, the droplet could not fully rebound or failed to rebound from **17F60%** surface at -15°C, attributed to the bigger surface roughness. When the temperature down to -25°C and -35°C, the droplet failed to rebound due to energy losses resulting from increased viscous. The ice shear strengths on all the prepared UV-curable film surfaces were lower than 210 kPa, only about 15% of the value on bare aluminum surface, which could be mainly attributed to the use of PDMS-SH. The UV-curable fluorosilicone triblock methacrylate copolymer films, especially for P17FMA-containing UV-curable films, which could not only prevent the freezing of impacting water droplet but also decrease the ice shear strength, have potential use as icephobic coatings.

Acknowledgements

This work is financially supported by National Natural Science Foundation of China (No. 51273146) and Natural Science Foundation of Tianjin, China (No. 14ZCZDGX00008).

Notes and references

1 C. C. Ryerson, *Cold. Reg. Sci. Technol.*, 2011, **65**, 97−110.
2 N. Dalili, A. Edrisy and R. Carriveau, *Renew. Sust. Energ. Rev.*, 2009, **13**, 428-438.
3 A. J. Meuler, J. D. Smith, K. K. Varanasi, J. M. Mabry, G. H. McKinley and R. E. Cohen, *ACS Appl. Mater. Interfaces*, 2010, **2**, 3100-3110.
4 M. Susoff, K. Siegmann, C. Pfaffenroth and M. Hirayama, Evaluation of icephobic coatings-screening of different coatings and influence of roughness, *Appl. Surf. Sci*., 2013, **182**, 870-879.
5 R. Dou, J. Chen, Y. Zhang, X. Wang, D. Cui, Y. Song, L. Jiang and J. Wang, *ACS Appl. Mater. Interfaces*, 2014, **6**, 6998-7003.
6 V. Hejazi, K. Sobolev and M. Nosonovsky, *Sci. Rep.*, 2013, **3**.
7 Y. Wang, J. Xue, Q. Wang, Q. Chen and J. Ding, *ACS Appl. Mater. Interfaces*, 2013, **5**, 3370–3381.
8 G. Momen and M. Farzaneh, *Appl. Surf. Sci.*, 2014, **299**, 41-46.
9 Y. Shen, J. Tao, H. Tao, S. Shen, L. Pan and Tao Wang, *RSC Adv*., 2015, **5**, 32813-32818.
10 T. Maitra, C. Antonini, M. K. Tiwari, A. Mularczyk, Z. Imeri, P. Schoch and D. Poulikakos, *Langmuir*, 2014, **30**, 10855-10861.
11 T. Maitra, M. K. Tiwari, C. Antonini, P. Schoch, S. Jung,; P. Eberle and D. Poulikakos, *Nano lett.*, 2013, **14**, 172-182.
12 T. Bharathidasan, S. V. Kumar, M.S. Bobji, R.P.S. Chakradhar and B. J. Basu, *Appl. Surf. Sci.*, 2014, **314**, 241-250.
13 H. A. Stone, *ACS Nano*, 2012, **6**, 6536–6540.
14 J. Chen, J. Liu, M. He, K. Li and D. Cu, *Appl. Phys. Lett.*, 2012, **101**, 111603.
15 S. Yang, Q. Xia, L. Zhu, J. Xue, Q. Wang and Q. Chen, *Appl. Surf. Sci.*, 2011, **257**, 4956-4962.
16 R. Menini and M. Farzaneh, *J. Adhes. Sci. Technol.*, 2011, **25**, 971-992.
17 K. Honda, M. Morita, O. Sakata, S. Sasaki and A. Takahara, *Macromolecules*, 2010, **43**, 454-460.
18 K. Honda, M. Morita, H. Otsuka and A. Takahara, *Macromolecules*, 2005, **38**, 5699-5705.
19 J. Yang, D. Yuan, B. Zhou, J. Gao, H. Ni, L. Zhang and X. Wang, *J. Colloid Interf. Sci.*, 2011, **359**, 269-278.
20 M. Morita, H. Ogisu and M. Kubo, *J. Appl. Polym. Sci.*, 1999, **73**, 1741-1749.
21 C. Wang, T. Fuller, W. Zhang and K. J. Wynne, *Langmuir*, 2014, **30**, 12819-12826.
22 D. Yu, Y. Zhao, H. Li, H. Qi, B. Li and X. Yuan, *Prog. Org. Coat.*, 2013, **76**, 1435-1444.
23 M. Niu, L. He, J. Liang, Aizhao. Pan and X. Zhao, *Prog. Org. Coat.*, 2014, **77**, 1603-1612.
24 J. Liang, L. He, X. Zhao, X. Dong, H. Luo and W. Li, *J. Mater. Chem.*, 2011, **21**, 6934.
25 C. Guan, Z. Luo, J. Qiu and P. Tang, *Eur. Polym. J.*, 2010, **46**, 1582-1593.
26 H. Murase, K. Nanishi, H. Kogure, T. Fujibayashi, K. Tamura and N. Haruta, *J. Appl. Polym. Sci.*, 1994, **54**, 2051-2062.
27 H. Murase and T. Fujibayashi, *Prog. Org. Coat.*, 1997, **31**, 97-104.
28 K. Zhang, J. Cai, X. Li, H. Li, Y. Zhao and X. Yuan, *Chinese J. Polym. Sci.*, 2015, **33**, 153-162.
29 H. Li, X. Li, C. Luo, Y. Zhao and X. Yuan, *Thin Solid Films*, 2014, **573**, 76-73.
30 X. Li, Y. Zhao, H. Li and Y. Xuan, *Appl. Surf. Sci.*, 2014, **316**, 222-231.
31 B. Li, X. Li, K. Zhang, H. Li, Y. Zhao, L. Ren and X. Yuan, *Prog. Org. Coat.*, 2015, **78**, 188-199.
32 C. Antonini, F. Villa, I. Bernagozzi, A. Amirfazli and M. Marengo, *Langmuir*, 2013, **29**, 16045−16050.
33 M. Wadley and K. Cavicchi, *J. Appl. Polym. Sci.*, 2010, **115**, 635-640.
34 Y. Mitsukami, M. Donovan, A. Lowe and C. McCormick, *Macromolecules*, 2001, **34**, 2248-2256.
35 S. Boileau, L. Bouteiller and A. Kowalewsk, *Polymer*, 2003, **44**, 6449-6455.
36 A. Orofino, M. Camezzana, M. Galante, P. Oyanguren and I. Zucchi, *Nanotechnology*, 2012, **23**, 115604.
37 H. Fang, S. Zhou and L. Wu, *Appl. Surf. Sci.*, 2006, **253**, 2978–2983.
38 M. Harvison, T. Davis and A. Lowe, *Polym. Chem*., 2011, **2**, 1347-1354.
39 Y. Wang, F. Liu and X. Xue, *Prog. Org. Coat.*, 2013, **76**, 863-869.
40 T. Uragmi, H. Yamada and T. Miyata, *Macromolecules*, 2006, **39**, 1890-1897.
41 P. Hartmann, A. Collet and M. Viguier, *Macromolecules*, 2006, **39**, 6975-6982.
42 H. Nakae, R. Inui, Y. Hirata and H. Staito, *Acta mater.*, 1998, **46**, 2313-2318.
43 S. T. Iacono, S. M.Budy, D. W. Smith, Jr and J. M. Mabry, *J. Mater. Chem*., 2010, **20**, 2979-2984.
44 V. Bahadur, L. Mishchenko, B. Hatton, J. Taylor, J. Aizenberg and T. Krupenkin, *Langmuir*, 2011, **27**, 14143-14150.
45 L. Mishchenko, B. Hatton, V. Bahadur, J. Taylor, T. Krupenkin and J. Aizenberg, *ACS nano*, 2010, **4**, 7699-7707.